machines

MDPI

Article

Adaptive Neuro-Fuzzy Control of Active Vehicle Suspension Based on H_2 and H_∞ Synthesis

Jaffar Seyyed Esmaeili [1], Ahmad Akbari [2], Arash Farnam [3,4,*], Nasser Lashgarian Azad [5] and Guillaume Crevecoeur [3,4]

[1] Department of Electrical Engineering, Atatürk University, Erzurum 25240, Turkey; jaffar.seyyedesmaeili17@ogr.atauni.edu.tr
[2] Department of Electrical Engineering, Sahand University of Technology, Tabriz 51335-1996, Iran; a.akbari@sut.ac.ir
[3] Department of Electromechanical, Systems and Metal Engineering, Ghent University, 9052 Ghent, Belgium; guillaume.crevecoeur@ugent.be
[4] Flanders Make@UGent-MIRO, 9052 Ghent, Belgium
[5] Department of Systems Design Engineering, University of Waterloo, Waterloo, ON N2L 3G1, Canada; nlashgar@uwaterloo.ca
* Correspondence: arash.farnam@ugent.be

Abstract: This paper addresses the issue of a road-type-adaptive control strategy aimed at enhancing suspension performance. H_2 synthesis is employed for modeling road irregularities as impulses or white noise, minimizing the root mean square (RMS) of performance outputs for these specific road types. It should be noted, however, that this approach may lead to suboptimal performance when applied to other road profiles. In contrast, the H_∞ controller is employed to minimize the RMS of performance outputs under worst-case road irregularities, taking a conservative stance that ensures robustness across all road profiles. To leverage the advantages of both controllers and achieve overall improved suspension performance, automatic switching between these controllers is recommended based on the identified road type. To implement this adaptive switching mechanism, manual switching is performed, gathering input–output data from the controllers. These data are subsequently employed for training an Adaptive Neuro-Fuzzy Inference System (ANFIS) network. This elegant approach contributes significantly to the optimization of suspension performance. The simulation results employing this novel ANFIS-based controller demonstrate substantial performance enhancements compared to both the H_2 and H_∞ controllers. Notably, the ANFIS-based controller exhibits a remarkable 62% improvement in vehicle body comfort and a significant 57% enhancement in ride safety compared to passive suspension, highlighting its potential for superior suspension performance across diverse road conditions.

Keywords: active suspension; H_2 synthesis; H_∞ synthesis; ride comfort; ride safety; ANFIS; LMI

Citation: Esmaeili, J.S.; Akbari, A.; Farnam, A.; Azad, N.L.; Crevecoeur, G. Adaptive Neuro-Fuzzy Control of Active Vehicle Suspension Based on H_2 and H_∞ Synthesis. *Machines* **2023**, *11*, 1022. https://doi.org/10.3390/machines11111022

Academic Editors: Zafer Bingul and Ferat Sahin

Received: 26 September 2023
Revised: 31 October 2023
Accepted: 9 November 2023
Published: 14 November 2023

1. Introduction

In the automotive industry, ensuring vehicle safety and passenger comfort are two primary design challenges. The vehicle suspension system plays a crucial role in achieving these objectives. It is responsible for isolating the vehicle body from vibrations and shocks caused by road surface irregularities to provide a smooth ride. Additionally, it should prevent the wheels from bouncing to maintain stable contact with the road for ride safety. However, these goals can conflict with one another. Improving ride comfort requires a larger suspension stroke, which means a soft suspension, while ride safety requires stiff damping. As a result, achieving the best possible passenger comfort without compromising road-holding requires adjusting these suspension parameters to suit different road profiles.

In passive suspension systems, the damper coefficient and spring stiffness are typically set during the design phase and cannot be adjusted to respond to different road profiles.

As a result, the development of more intelligent suspension systems, such as semi-active and active suspension systems, has become increasingly popular within the automotive industry and academic communities. These advanced suspension systems provide the capability to adjust the suspension parameters in real time to adapt to changing road conditions, resulting in improved ride comfort and safety.

The active suspension system employs a singular linear electromagnetic or hydraulic actuator, paired with its respective amplifier, at each corner of the vehicle. This configuration has the capability to either replace or function concurrently with the conventional damper–spring setup. In the last decade, several control methodologies have emerged for the enhancement of active suspension systems, including robust control [1–6], preview-based active suspension [7–9], optimal control [9–12], and adaptive control [4,13–16]. Since neural networks and fuzzy controls are the key branches of intelligent control, numerous studies have been conducted on using adaptive control methods, neural networks, and fuzzy control theory to control active suspension systems [17–21]. These approaches have been shown to improve ride comfort and handling performance by adapting to changing road conditions and providing real-time control of suspension dynamics, either independently or in conjunction with complementary methodologies [16,22–25]. Two additional prominent methodologies that have been extensively studied in the existing literature include Model Predictive Control (MPC) and Sliding Mode Control (SMC). MPC excels in dynamic adaptation through predictive modeling, resulting in improved ride comfort and vehicle handling, while SMC showcases robustness to uncertainties and disturbances, enhancing stability and control precision in suspension applications. In both cases, substantial performance improvements have been consistently observed when compared to passive suspension systems, affirming the effectiveness of these control methodologies [26–30].

In the domain of vibration analysis, researchers often model road surface irregularities as a stochastic process. This involves characterizing them either as white noise ground speed or as deterministic disturbances, such as road bumps or puddles acting as impulse inputs [31]. The H_2 norm, serving as a quantitative measure of the root mean square (RMS) amplitude of the system's output in reaction to white noise or impulse inputs, is a prevalent metric employed for the evaluation of ride comfort within the context of vehicular dynamics analysis [10]. Consequently, the H_2 norm is frequently regarded as the preferred option, as it is typically less conservative than the H_∞ norm when quantifying ride comfort in scenarios where the system is subjected to white noise or impulse inputs. As a result, many researchers have explored the use of Linear Quadratic Gaussian (LQG) and H_2 norm minimization in the design of active vehicle suspension systems [2,31–33].

It is crucial to emphasize that the efficacy of H_2 synthesis can diminish when the suspension system encounters road profiles different from those it was initially designed for, especially in cases where the road inputs are deterministic, such as bumps or potholes. On the other hand, H_∞ control is designed to minimize the RMS value of the system output for worst-case road irregularities, ensuring a conservative approach that is effective for all road profiles, including deterministic inputs. As a result, numerous studies on H_∞ or μ synthesis have been conducted in the field of suspension design, including [1,7,8] and [34–36].

To enhance the performance of the suspension system in response to a wide range of road irregularities, our novel approach recommends automatic controller switching contingent upon the road type. This is achieved through meticulous manual controller transitions and the systematic accumulation of input–output datasets from diverse road profiles. The resulting dataset serves as the foundation for training an innovative Adaptive Neuro-Fuzzy Inference System (ANFIS) controller. The main novelties of this work can be summarized as follows:

- Dynamic Controller Transition and Data Collection: The proposed methodology introduces dynamic switching between controllers based on road characteristics, a novel approach for improving suspension system performance. An emphasis on meticulous manual controller transitions and comprehensive data collection across various

road profiles distinguishes this approach, paving the way for data-driven suspension optimization. The combination of fuzzy logic and neural network techniques allows the ANFIS controller to provide continuous and smooth control actions as the input conditions change. This smooth transition helps avoid sudden changes in control output, which can contribute to system stability and improved performance.

- Pioneering Utilization of ANFIS Controller as a Hybrid Controller Training Approach: One of the key innovations in this research is the training of the ANFIS controller using input–output data from both the H_2 and H_∞ controllers. This hybrid training approach leverages the knowledge and performance characteristics of both controller types to enhance the capabilities of the ANFIS controller, resulting in a unique and powerful control system for suspension optimization.

The structure of this study is outlined as follows: In Section 2, a detailed description of the quarter-car model used for the suspension system in this paper is presented. Additionally, this section elaborates on the active control problem, providing specific details regarding the control objectives aimed at enhancing ride safety and comfort. Section 3 introduces the linear matrix inequality (LMI)-based H_2 and H_∞ control methods as the foundation for designing the ANFIS-based controller structure. This section also outlines the ANFIS neuro-fuzzy architecture. Section 4 contains simulation studies, which serve to illustrate the effectiveness and advantages of the proposed method in achieving the control objectives when compared to the two previously employed control approaches. Lastly, in Section 5, concluding remarks are provided.

2. Problem Formulation and Design Method

2.1. Quarter-Car Model

In this study, a 2-degree-of-freedom (2-DOF) quarter-car model is employed to depict the suspension system, as illustrated in Figure 1. This model comprises two main components: the chassis, denoted as the sprung mass (m_s), and the axle, referred to as the unsprung mass (m_u). A suspension system is mounted between these components to facilitate the analysis. This model is widely used in active vehicle suspension studies due to its ability to effectively capture the essential characteristics of a real suspension system.

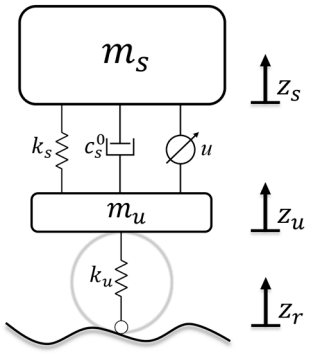

Figure 1. Quarter-car model of the active suspension system.

The equations of motion that elucidate the behavior of the sprung and unsprung masses in the active suspension system are expressed as follows:

$$m_s\ddot{z}_s = k_s(z_u - z_s) + b_s(\dot{z}_u - \dot{z}_s) + u \tag{1}$$

$$m_u\ddot{z}_u = k_s(z_s - z_u) + b_s(\dot{z}_s - \dot{z}_u) + k_u(z_r - z_u) - u \tag{2}$$

where z_s and z_u represent the displacement of the sprung and unsprung masses, while k_s and k_u signify the spring constant of the suspension system and the tire stiffness, respectively; b_s is indeed the damping coefficient of the suspension system; z_r is the road disturbance input; and u signifies the control input.

The state variables are chosen as follows:

$$x_1(t) = z_s - z_u$$

$$x_2(t) = z_u - z_r$$

$$x_3(t) = \dot{z}_s$$

$$x_4(t) = \dot{z}_u$$

The state-space representation of the quarter-car model is provided below:

$$\dot{x}(t) = Ax(t) + B_1 w(t) + B_2 u(t)$$

with

$$A = \begin{bmatrix} 0 & 0 & 1 & -1 \\ 0 & 0 & 0 & 1 \\ -\frac{k_s}{m_s} & 0 & -\frac{c_s}{m_s} & \frac{c_s}{m_s} \\ \frac{k_s}{m_u} & -\frac{k_u}{m_u} & \frac{c_s}{m_u} & -\frac{c_s}{m_u} \end{bmatrix}, \; B_1 = \begin{bmatrix} 0 & 0 & 0 \\ -1 & 0 & 0 \\ 0 & 0 & 0 \\ 0 & 0 & 0 \end{bmatrix}, \quad B_2 = \begin{bmatrix} 0 \\ 0 \\ \frac{1}{m_s} \\ -\frac{1}{m_u} \end{bmatrix}$$

The road roughness-induced disturbance input is denoted as $w = \dot{z}_r$. The parameter values employed in this study are presented in Table 1 [37].

Table 1. Parameters of "Renault Mégane Coupe" car.

Symbol	Description	Value
m_s	Sprung mass	315 kg
m_u	Unsprung mass	37.5 kg
k_s	Suspension stiffness	29,500 N/m
k_u	Tire stiffness	210,000 N/m
b_s	Suspension damping coefficient	1500 N·s/m
$\left[\underline{z}_{def}, \overline{z}_{def}\right]$	Suspension deflection limits	$[-8, 6]$ cm

2.2. Design Objectives

The assessment of body acceleration serves as a prevalent metric in evaluating passenger comfort within vehicular contexts. In the pursuit of enhancing passenger comfort, it becomes imperative to minimize both the vertical displacement and the rate of change in velocity (acceleration) experienced by the vehicle's body. This objective can be effectively pursued through the optimization of damper displacement. The role of dampers, also known as shock absorbers, in this endeavor, is pivotal. Dampers, as integral components of a vehicle's suspension system, significantly contribute to mitigating the effects of road irregularities on passenger comfort. Notably, the damper force exerted depends on the vehicle's speed, increasing in magnitude as the vehicle's speed rises. This modulation of damper force with speed is essential to effectively control and dampen body movements, maintaining both ride comfort and road-holding capabilities.

However, it is paramount to underscore that safety represents an equally essential consideration alongside comfort. Ensuring safe driving conditions necessitates the maintenance of optimal tire-to-road contact. Consequently, the design of the suspension system must be executed with meticulous attention to balance the dual imperatives of comfort and safety under various driving scenarios, all while considering the dynamic fluctuations in system parameters.

In designing a controller for a suspension system, the following specifications must be taken into account:

- Ride comfort: Ride comfort is commonly assessed by quantifying the RMS value of acceleration experienced by passengers [7]. To attain optimal ride comfort, it is

imperative to minimize this value to the greatest extent possible within the frequency range of passenger body sensitivity, typically falling between 1 Hz and 8 Hz [31]. When road roughness is predominantly modeled as white noise or impulse input (as is frequently the case), enhancing ride comfort involves the minimization of the H_2 norm of the transfer function from road displacement to chassis acceleration ($\ddot{z}_s$), with appropriate weighting applied to the relevant frequencies. However, if the road disturbances include more complex waveforms than white noise (such as deterministic patterns), achieving optimal ride comfort may require the use of H_∞ performance.

- Road-holding: To achieve good road-holding, it is necessary to maintain continuous contact between the tires and the road surface. In the context of a given road profile, this objective can be accomplished by minimizing the H_2 or H_∞ norms of the transfer function from the road disturbance to tire displacement ($z_{ur} = z_u - z_r$). It is essential to emphasize that maintaining rigid contact between the tires and the road necessitates that the dynamic tire load does not surpass the static load [14], i.e.,

$$k_u(z_u - z_r) < (m_s + m_u)g, \qquad \forall\, t \geq 0$$

  This fact can be utilized to normalize the dynamic tire load.
- Suspension stroke limits: Suspension deflection (z_{def}) plays a crucial role in achieving the required road-holding specifications, and it is imperative to maintain the deflection limits to ensure optimal ride comfort and prevent any structural damage to the system. As a result, it becomes imperative to confine the transfer function z_{def}/z_r within the established upper and lower bounds to achieve the desired outcomes. Deviating from these limits can result in compromised ride comfort and have an adverse impact on the overall performance of the vehicle. To avoid excessive suspension bottoming, it has to consider the limitations of suspension deflection and incorporate appropriate measures to maintain optimal performance, as follows:

$$|z_{def}| = |z_s - z_u| \leq z_{def_{max}}$$

- Control signal: The control signal is produced by a hydraulic actuator and is constrained due to its saturation. It is hypothesized that the normalized control signal is bounded, as expressed by the inequality:

$$|u| < u_{max}$$

In order to optimize ride comfort, it is essential to minimize the RMS value of body acceleration, all the while allowing suspension deflection, tire deflection, and the control signal to fluctuate within their pre-defined limits.

Due to the predominant modeling of road roughness as white noise [31], the H_2 norm appears to be less cautious than the H_∞ norm when quantifying any of the aforementioned outputs. Moreover, in the suggested approach, the H_∞ controller is employed to achieve robust performance goals and ride stability by minimizing the associated transfer functions for road disturbances that are more inclusive than just white noise and impulse. In light of these factors, it is evident that there is a requirement for a controller that encompasses all of the aforementioned features of both controllers.

2.3. Review of H_2 and H_∞ Design Frameworks

2.3.1. H_2 Synthesis

The control objectives outlined in the preceding section necessitate the incorporation of normalizing weights into both control outputs $\left[z_{def}\ z_{ur}\ \ddot{z}_s\right]$ and exogenous inputs $[w\ n_1\ n_2]$. Figure 2 depicts a general block diagram of the system. As mentioned earlier, it is crucial to identify specific frequency conditions concerning suspension deflection (aiming to reduce gain at lower frequencies), dynamic tire load, and the control signal. Input weights denote the frequency characteristics of the inputs, while output weights

signify the desired frequency components of the controlled outputs [32]. Additionally, it is crucial to acknowledge the presence of measurement noise, denoted as n_1 and n_2, which can affect the accuracy of the measured outputs $y = [y_1\ y_2]$. The practical importance of these measured outputs, specifically suspension deflection and body acceleration, cannot be overstated. They can be readily acquired through the utilization of suitable sensors. Therefore, the inclusion of normalizing weights accounts for the frequency characteristics of both inputs and measurements, contributing to the effective control of the system while considering these exogenous noise inputs in the design procedure.

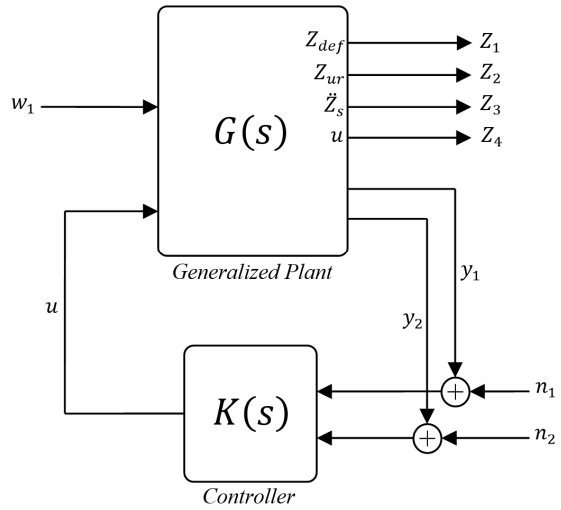

Figure 2. Generalized block diagram of the active suspension system.

The following is a description of the augmented plant model for the design:

$$\begin{aligned} \dot{x}(t) &= Ax(t) + B_1 w(t) + B_2 u(t) \\ z(t) &= C_1 x(t) + D_{11} w(t) + D_{12} u(t) \\ y(t) &= C_2 x(t) + D_{21} w(t) + D_{22} u(t) \end{aligned} \tag{3}$$

The core aim is to develop an H_2 controller that guarantees the stability of the closed-loop system while meeting specific control objectives. These objectives encompass reducing the H_2 norm between the disturbance input ω and two key variables: body acceleration ($\ddot{z}_s$) and tire deflection (z_{ur}). This optimization aims to enhance ride comfort and ride safety, respectively. Simultaneously, the control signal (u) and suspension deflection (z_{def}) must be maintained within their allowable boundaries. The choice of weights is made to align with the design framework within the specified frequency range.

For the H_2 design, let us describe the controller as follows:

$$K := \begin{pmatrix} \dot{x}_c \\ u \end{pmatrix} = \begin{pmatrix} A_c & B_c \\ C_c & D_c \end{pmatrix} \begin{pmatrix} x_c \\ y \end{pmatrix} \tag{4}$$

The state-space representation of the closed-loop system is obtained as follows:

$$\begin{aligned} \mathcal{A}_{cl} &:= \begin{pmatrix} A + B_2 D_c C_2 & B_2 C_c \\ B_c C_2 & A_c \end{pmatrix} \\ \mathcal{B}_{cl} &:= \begin{pmatrix} B_1 + B_2 D_c D_{21} \\ B_c D_{21} \end{pmatrix} \\ \mathcal{C}_{cl} &:= \begin{pmatrix} C_1 + D_{12} D_c C_2 & D_{12} C_c \end{pmatrix} \\ \mathcal{D}_{cl} &:= D_{11} + D_{12} D_c D_{21} \end{aligned} \tag{5}$$

Theorem 1. *The closed-loop system will be stable, and the H_2 norm from exogenous inputs to controlled outputs will be less than γ if, and only if, there exist symmetric positive definite matrices, $\mathcal{X}$ and $\mathcal{Z}$, that satisfy the following inequalities [33]:*

$$\begin{pmatrix} \mathcal{A}_{cl}\mathcal{X} + \mathcal{X}\mathcal{A}_{cl}^T & \mathcal{B}_{cl} \\ * & -I \end{pmatrix} \prec 0$$
$$\begin{pmatrix} \mathcal{Z} & \mathcal{C}_{cl}\mathcal{X} \\ * & \mathcal{X} \end{pmatrix} \succ 0 \tag{6}$$
$$Trace(\mathcal{Z}) < \gamma^2, \quad \mathcal{D}_{cl} = 0$$

2.3.2. H_∞ Synthesis

The primary objective of H_∞ controller design is to minimize the H_∞ norm of a system while preserving internal stability [38]. It is worth noting that the H_∞ norm possesses diverse interpretations, particularly concerning its application in both the time and frequency domains. In the frequency domain, the objective is to diminish the peak singular value of the transfer function concerning frequency. This goal equates to minimizing the system's maximum gain across the entire frequency spectrum:

$$\|G(s)\|_\infty \triangleq \sup_\omega \overline{\sigma}(G(j\omega)) \tag{7}$$

In the single-input, single-output (SISO) scenario, the H_∞ norm is synonymous with the maximum magnitude of the transfer function. The H_∞ norm's interpretation in the time domain is expressed as the induced 2-norm, as detailed below [39]:

$$\|G(s)\|_\infty = \sup_{w(t)\neq 0} \frac{\|z(t)\|_2}{\|w(t)\|_2} \tag{8}$$

where the induced 2-norm, indicated as $\|z(t)\|_2 = \sqrt{\int_0^\infty \sum_i |z_i(t)|^2 dt}$, signifies the energy content of the signal vector. In the context of the time domain interpretation of the H_∞ norm, the primary objective is to mitigate the energy of the output signal when subjected to the most adverse input signal conditions.

In accordance with the principles of linear dissipative systems, the controller can be derived by satisfying the bounded realness condition, commonly referred to as the bilinear matrix inequality (BMI) [40]:

$$\textit{Minimize } \gamma_\infty \textit{ subject to}$$
$$\boldsymbol{\mathcal{X}} \succ 0 \tag{9}$$
$$\begin{pmatrix} \mathcal{A}_{cl}^T K + K\mathcal{A}_{cl} & K\mathcal{B}_{cl} & \mathcal{C}_{cl}^T \\ * & -\gamma_\infty^2 I & \mathcal{D}_{cl}^T \\ * & * & -I \end{pmatrix} \succ 0$$

By employing a change in variables similar to the H_2 design and an appropriate congruence transformation, the corresponding LMI (linear matrix inequality) conditions for H_∞ can be obtained. The Appendix A is devoted to this transformation. Also, readers are encouraged to refer to [41,42] for a more detailed understanding of this process.

3. Adaptive Neuro-Fuzzy Inference Systems (ANFIS)

For simplicity, a fuzzy system architecture, commonly known as the Type-3 ANFIS structure, is considered with a two-input, two-rule fuzzy system that accommodates five layers inside it [43]. Suppose that two if–then rules of a Sugeno-type fuzzy system are as given below:

$$\text{If } x \text{ is } A1 \text{ and } y \text{ is } B1, \text{ then } f_1 = p_1 x + q_1 y + r_1$$

$$\text{If } x \text{ is } A2 \text{ and } y \text{ is } B2, \text{ then } f_2 = p_2 x + q_2 y + r_2$$

The equivalent ANFIS structure corresponding to this controller design is illustrated in Figure 3. The node functions within a given layer are members of the same function family, and this family is described as follows:

- Layer 1: Every node in this layer is depicted as a square shape, each associated with a specific membership function:
$$O_i^1 = \mu_{A_i}(x)$$
where the superscripts above and below denote the layer number and the node index within the layer, respectively. The input to the i-th node in this layer is denoted by x (or y), while A_i represents the corresponding linguistic term associated with this node (e.g., "small", "large", etc.). In this specific case, the membership function, denoted as $\mu_{A_i}(x)$, is selected to have a bell-shaped form with a maximum value of 1 and a minimum value of 0, as illustrated below:
$$O_i^1 = \mu_{A_i}(x) = \frac{1}{1 + \left[\left(\frac{x - c_i}{a_i}\right)^2\right]^{b_i}} \tag{10}$$
The parameter set $\{a_i, b_i, c_i\}$ corresponds to the specific parameters of the bell-shaped membership function. Any variation in the values of these parameters will result in changes to the shape of the bell-shaped function accordingly. As a result, a wide range of membership functions can be induced for the linguistic value A_i by adjusting the values of these parameters.
- Layer 2: Each node in this layer is represented by a circular shape denoted by the symbol Π, indicating that the incoming signals are multiplied. The output of the node is calculated as the T-norm (logical AND) multiplication of the input signals, as follows:
$$O_i^2 = w_i = \mu_{A_i}(x) \times \mu_{B_i}(y), \quad i = 1, 2$$
where $\mu_{A_i}(x)$ and $\mu_{B_i}(y)$ are the membership functions for the input variables x and y, respectively, associated with the i-th node, and $\times$ represents the logical AND operator. The resulting value w_i represents the firing strength or degree of membership for the i-th rule. Each output node corresponds to the firing strength of a specific rule.
- Layer 3: Every node within this layer is a fixed node, symbolized by a circular shape marked as N. This layer executes a normalization procedure involving summation and arithmetic division. Specifically, the i-th node computes the ratio of the i-th rule's firing strength to the total sum of all rules' firing strengths, as follows:
$$O_i^3 = \overline{w}_i = \frac{w_i}{w_1 + w_2}, \; i = 1, 2$$
The computed values, denoted as $\overline{w}_i$, are termed normalized firing strengths. These values signify the extent of the contribution of each rule towards the ultimate output of the ANFIS model.
- Layer 4: Each node in this layer is represented by a square shape and performs the multiplication of the normalized output of layer 3, $\overline{w}_i$, with the "then" part of the fuzzy rule, denoted as f_i, as follows:
$$O_i^4 = \overline{w}_i f_i = \overline{w}_i (p_i x + q_i y + r_i)$$
The set of parameters $\{p_i, q_i, r_i\}$ are referred to as the consequent parameters, and they determine the shape and position of the output surface of the ANFIS model.

- Layer 5: The presented neural network architecture comprises a single node characterized by a circular shape and identified as Σ. The output of this layer is calculated through the algebraic summation of the input signals, represented as follows:

$$O_1^5 = \sum_{i=1}^{2} \overline{w}_i f_i = \frac{\sum_{i=1}^{2} \overline{w}_i f_i}{\sum_{i=1}^{2} w_i} \tag{11}$$

Here, w_i and f_i denote the weight and input signal of the i-th input node, respectively. The output O_1^5 represents the weighted sum of the input signals normalized by the sum of the weights.

In this way, a Type-3 ANFIS structure is established, demonstrating functional equivalence to a Type-3 fuzzy reasoning system.

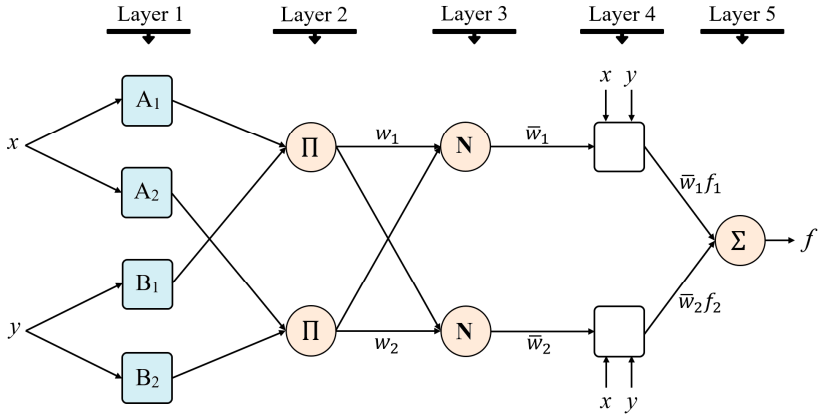

Figure 3. Type-3 ANFIS architecture.

ANFIS Design

The ANFIS algorithm utilizes input–output datasets obtained from the design procedure of the H_2 and H_∞ controllers to construct a fuzzy inference system (FIS). To generate a training dataset for the ANFIS controller in an active suspension system, data were collected for both the H_2 and H_∞ controllers by simulating the vehicle over various road conditions while recording the input parameters (e.g., road roughness) and the corresponding output control actions from each controller. We labeled the data to indicate which controller was active during data collection. Specifically, the training data used as input to the ANFIS system comprised the deflection and acceleration of the suspension system, while the output data were generated from two distinct sources: The first component of the output data is related to the command force data generated by the H_∞ controller in response to the bump, which is designed to enhance the robustness of the system. The second component of the output data is linked to the force command of the H_2 controller in response to the white noise road profile. The data were collected over a period of 10 s for each controller, resulting in a total of 60,000 data points. To train the ANFIS system, the first 70% of the data were used as the training dataset, while the remaining 30% were reserved for validating the system. ANFIS automatically determines when to switch smoothly between controllers during inference by evaluating the input conditions and the learned knowledge from the dataset. This allows it to make dynamic controller transitions for optimal suspension performance, as it continuously adjusts its output based on the current road conditions and the knowledge it has acquired from the training data. In this study, we analyze the response of closed-loop systems to an asphalt road profile comprising white noise and bump disturbance. For the purpose of this study, we define bump disturbance as follows:

$$z_r(t) = \begin{cases} \frac{h}{2}\left(1 - cos\left(\frac{2\pi v t}{l}\right)\right) & , \quad 0 \le t \le \frac{l}{v} \\ 0 & , \quad t > \frac{l}{v} \end{cases} \tag{12}$$

Bump disturbance is described using the following parameters: h = 0.1 m, l = 2 m, and v = 10 m/s (equivalent to 36 km/h); these represent the height and length of the bump, and the velocity of the vehicle, respectively. Figures 4 and 5 illustrate the training data and validation results for the command force of both types of road inputs, along with their respective errors. Specifically, Figures 4a and 5a depict the predicted command force and its ability to track the target command force, while Figure 4b,c and Figure 5b,c present the corresponding error and its RMS value, respectively. These results demonstrate that the ANFIS system is capable of accurately predicting the command force, as evidenced by the small magnitude of the error and its RMS value.

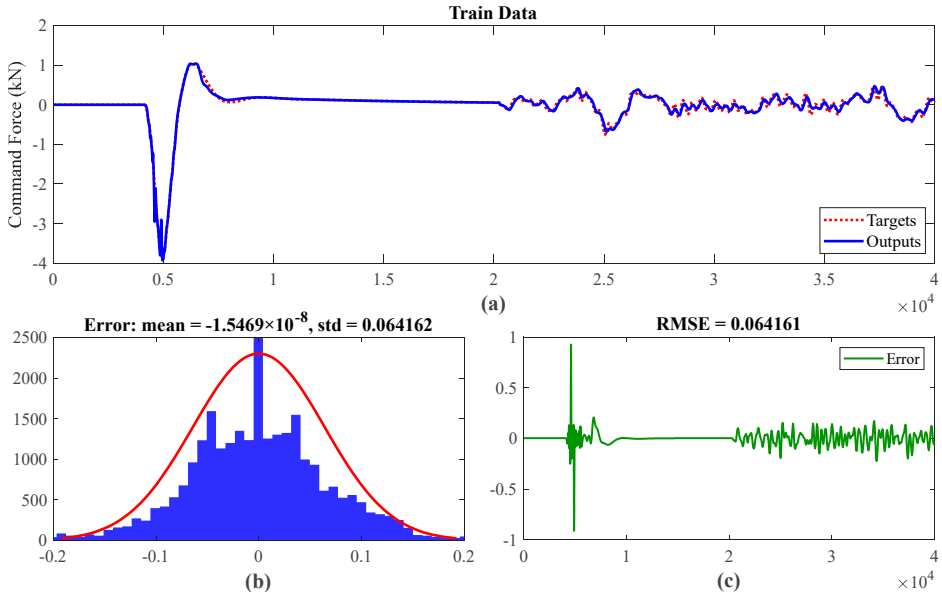

Figure 4. (**a**) Training data, (**b**) training error, and (**c**) training RMSE.

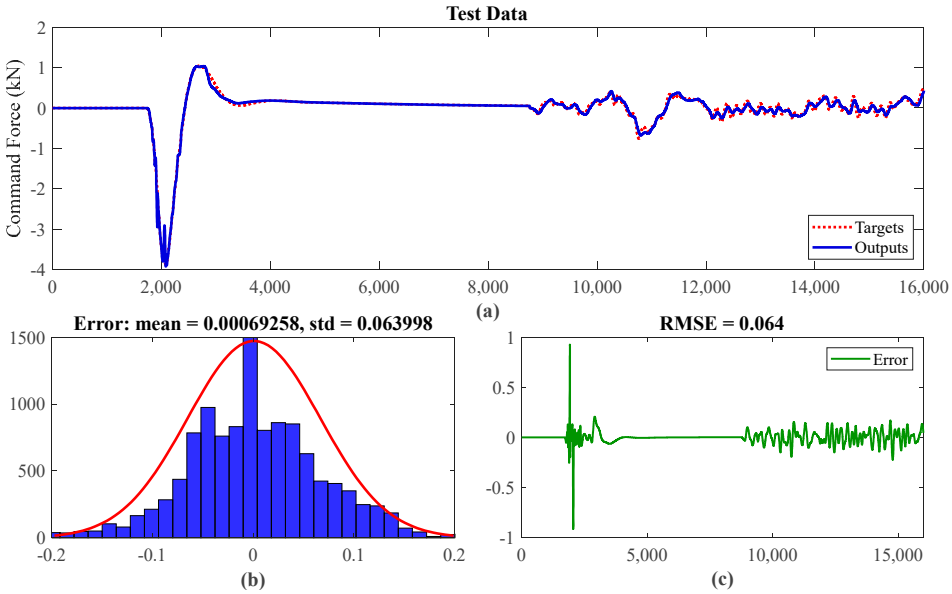

Figure 5. (**a**) Test data, (**b**) test error, and (**c**) test RMSE.

4. Simulation Results

The design procedures for the H_2 and H_∞ controllers were performed separately, following the steps outlined in [32]. The simulations were conducted in the 2020b MATLAB/Simulink environment. In order to assess the effectiveness of the H_2 and H_∞ controllers, a comparative analysis was conducted by examining the frequency response of

the desired objectives in contrast to that of a passive suspension system across a broad frequency spectrum, as depicted in Figure 6. The results indicate a significant improvement in body acceleration and tire deflection for both controllers. As mentioned before, the H_2 controller is designed to minimize the mean squared value (L_2 norm) of the system's output, which equates to reducing energy or power within specific frequency bands. This design characteristic renders the H_2 controller especially adept at mitigating vibrations. In the realm of active suspension systems, where vibrations within the 1 to 20 Hz frequency range significantly influence ride comfort and road handling, the H_2 controller excels by effectively managing vibrations within this critical frequency range, thereby underpinning its superior performance in this context.

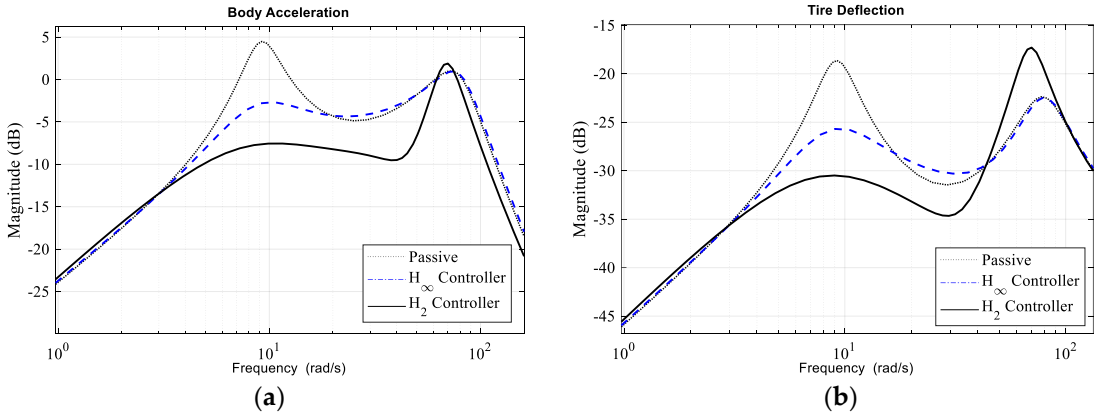

Figure 6. Frequency responses: (**a**) body acceleration, (**b**) tire deflection.

In Figure 7, a comparison is presented illustrating the weighted body acceleration responses for both H_2 and H_∞ controllers when subjected to bump and asphalt road inputs. The findings reveal that the H_2 controller excels in minimizing body acceleration and tire deflection under asphalt road input, whereas the H_∞ controller outperforms the H_2 controller in response to bump input. This observation underscores the distinct strengths and weaknesses inherent in each controller. Therefore, the selection of the appropriate controller hinges on the specific road conditions and the defined design objectives.

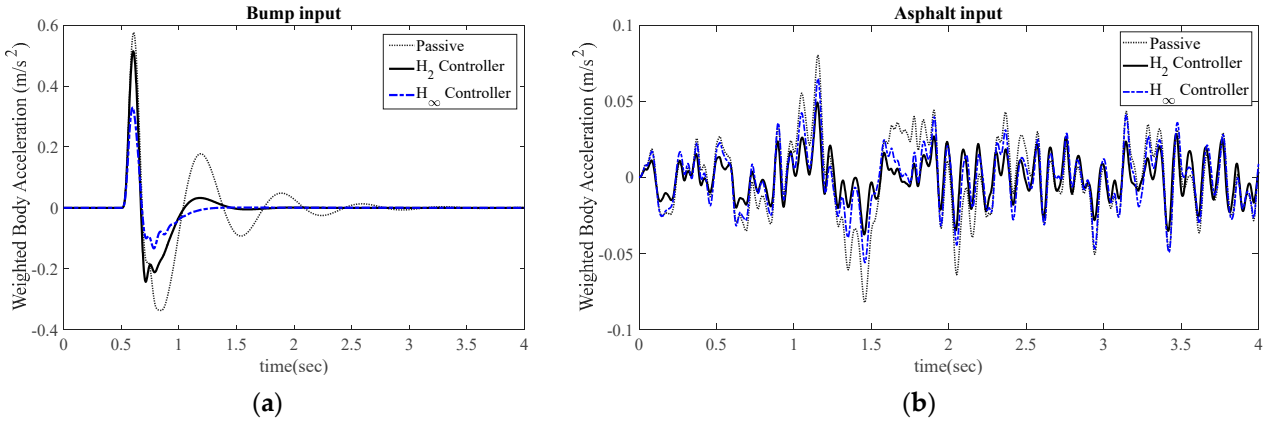

Figure 7. Comparison of body acceleration of H_2 and H_∞ controllers: (**a**) bump input, (**b**) real-world asphalt road.

Based on the aforementioned details, the proposed ANFIS-based controller is anticipated to incorporate the desirable properties of both the H_2 and H_∞ controllers in response to road inputs. To evaluate the effectiveness of the proposed ANFIS-based controller, a comparison was conducted with the two aforementioned controllers in terms of body acceleration and tire deflection. These parameters serve as key indicators in suspension

design, significantly influencing both ride safety and comfort. These comparisons are presented in Figure 8, with the road profile consisting of a real-world asphalt road profile with two tandem bumps. As demonstrated in Figure 8, the proposed ANFIS-based controller outperforms both the H_2 and H_∞ approaches in terms of meeting the design objectives. Specifically, the proposed method achieves the best performance in minimizing body acceleration and tire deflection, thereby improving ride safety and comfort. In other words, the ANFIS-based controller behaves like the H_∞ controller when confronted with the bump input, while it behaves like the H_2 controller in response to the asphalt road input. This property of the ANFIS-based controller allows it to achieve optimal performance under both types of road inputs. It thus represents a significant improvement over either the H_2 or H_∞ controller alone.

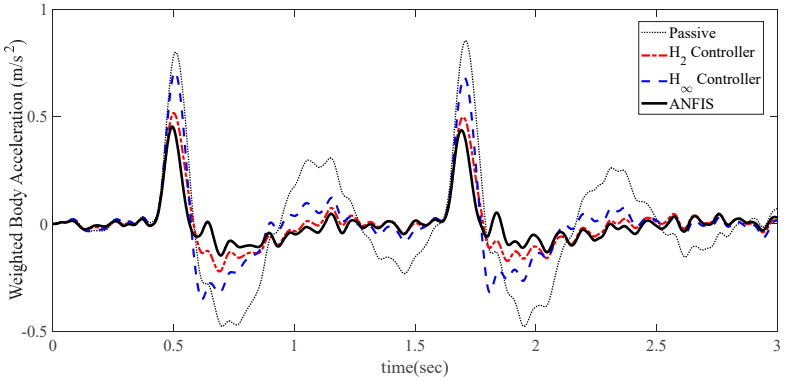

(**a**)

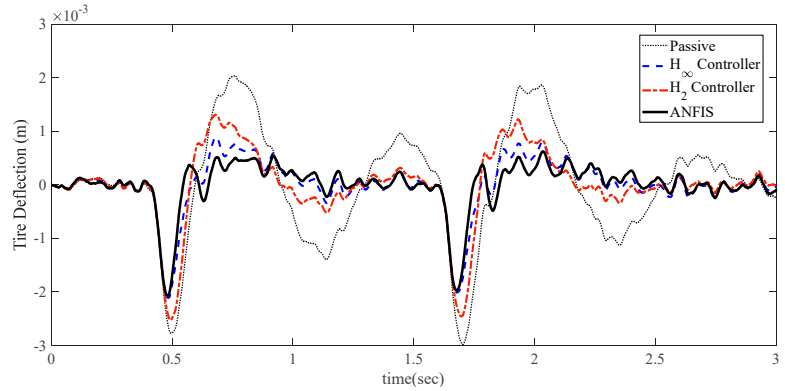

(**b**)

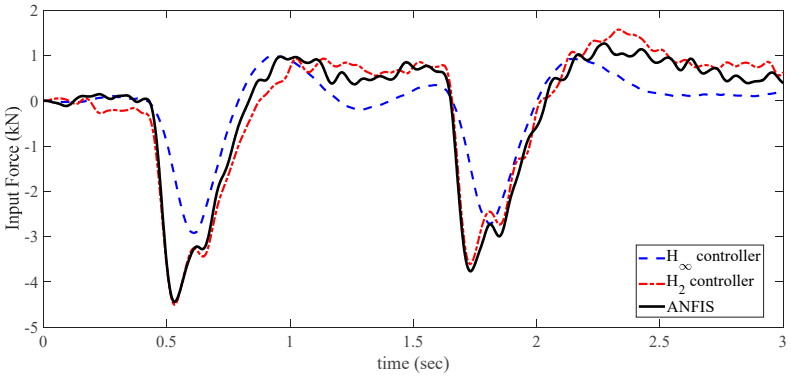

(**c**)

Figure 8. Comparison of the proposed ANFIS controller with H_2 and H_∞ controllers: (**a**) weighted body acceleration, (**b**) tire deflection, (**c**) input force.

The RMS values of the design objectives are listed in Table 2 to compare the three methods.

Table 2. RMS values of design objectives.

System	$\ddot{z}_s$ (m/s^2)	z_{ur} (m)	z_{def} (m)	Force (kN)
Passive	0.203	8.1×10^{-4}	0.103	0
H_2 controller	0.097	5.33×10^{-4}	0.091	1.51
H_∞ controller	0.138	4×10^{-4}	0.073	1.20
ANFIS	0.077	3.5×10^{-4}	0.97	1.40

In this comparative study of active suspension systems, we evaluated performance based on key design objectives (body acceleration ($\ddot{z}_s$), suspension deflection (z_{def}), and unsprung mass displacement (z_{ur})) using RMS values. The ANFIS-based controller emerges as the standout performer, achieving a remarkable 62.07% reduction in body acceleration and a significant 56.8% decrease in unsprung mass displacement compared to the passive suspension. The ANFIS-based controller exhibits a slight decrease of 5.83% in suspension deflection compared to the passive system.

Comparatively, when assessed against the H_2 controller, ANFIS demonstrates a 20.6% improvement in body acceleration, a substantial 34.33% reduction in unsprung mass displacement, a modest 6.6% increase in suspension deflection, and a slight 7% decrease in command force.

Similarly, when compared to the H_∞ controller, ANFIS excels with a 44.2% reduction in body acceleration and a 42.9% increase in suspension deflection. Additionally, ANFIS reduces unsprung mass displacement by 12.5% and increases command force by 16.7%. Importantly, it is noteworthy that the ANFIS-based controller, while exhibiting slightly increased suspension deflection compared to the H_2 and H_∞ controllers, still operates well within the predefined structural limitations of the suspension system deflection. This controlled increase in suspension deflection ensures that the system maintains stability and structural integrity within acceptable structural constraints.

In summary, these outcomes affirm the effectiveness of the proposed ANFIS-based controller in meeting the design goals of enhancing ride comfort and safety. Additionally, it ensures that suspension stroke and command force remain within their predetermined limits. Notably, the ANFIS-based controller exhibits distinct advantages over the H_2 and H_∞ controllers, particularly in the reduction of body acceleration and unsprung mass displacement. This makes ANFIS a compelling choice for improving active suspension system effectiveness while ensuring structural integrity within defined constraints. These improvement percentages are illustrated in Figure 9. It is important to acknowledge that in this comparison, the passive suspension system serves as the baseline. Consequently, the force section is omitted from the plotted data.

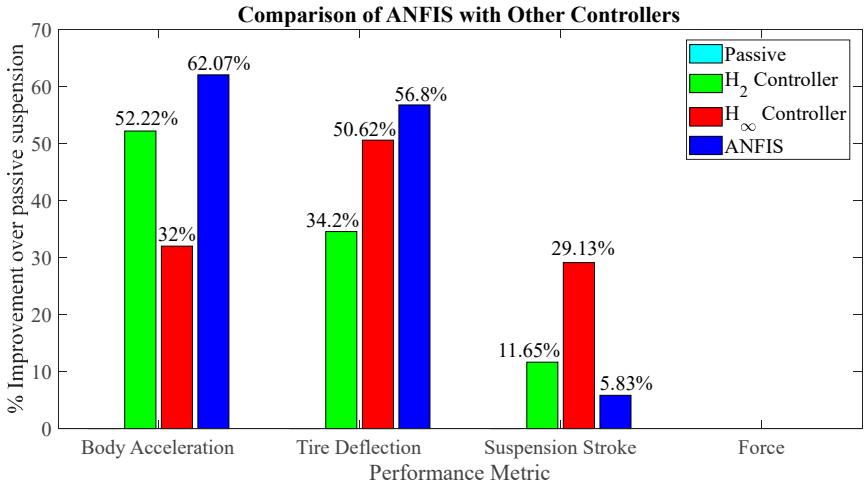

Figure 9. Comparison of ANFIS-based control performance with other controllers over passive suspension.

5. Conclusions

In this research endeavor, we introduced an Adaptive Neuro-Fuzzy Inference System (ANFIS)-based controller as a novel approach to the design of active vehicle suspension systems. This ANFIS controller was formulated to encompass the comprehensive attributes associated with both H_2 and H_∞ controllers, specifically emphasizing optimizing ride comfort and ensuring safety.

The ANFIS methodology was carefully employed to construct a fuzzy inference system, utilizing input–output datasets derived from the distinct design methodologies employed in H_2 and H_∞ controllers. The ensuing simulation results, employing a quarter-car model, were meticulously compared with those obtained using the H_2 and H_∞ controllers. Our investigation has unequivocally demonstrated that the ANFIS-based controller offers substantial performance advantages, achieving optimal ride comfort while effectively constraining suspension deflection and control force within their prescribed limits, thus concurrently upholding ride safety standards. Ultimately, our findings underscore the potential efficacy and efficiency of the ANFIS-based controller as a compelling solution in the domain of active vehicle suspension system design. This research presents a significant stride toward enhancing vehicular ride quality and safety through advanced control methodologies.

In future work, optimizing the ANFIS-based controller, evaluating its robustness under uncertainties, and validating its performance through practical experiments are essential steps for assessing its application and real-time performance.

Author Contributions: Conceptualization and methodology, J.S.E. and A.A.; software, J.S.E.; validation, J.S.E., A.A. and A.F.; formal analysis, J.S.E., A.A. and A.F.; investigation and data curation, J.S.E.; writing—original draft preparation, J.S.E.; writing—review and editing, A.A., A.F., N.L.A. and G.C.; visualization, J.S.E.; supervision, A.A., A.F., N.L.A. and G.C. All authors have read and agreed to the published version of the manuscript.

Funding: This research is part of the DIRAC SBO project funded and supported by Flanders Make.

Data Availability Statement: The authors confirm that the data supporting the findings of this study are available within the article.

Conflicts of Interest: The authors declare no conflict of interest.

Appendix A

According to linear dissipative systems theory, a closed-loop H_∞ controller is obtained by solving the following Bounded Real Lemma (BRL):

$$\begin{bmatrix} \mathcal{A}^T K + K\mathcal{A} & K\mathcal{B} & \mathcal{C}^T \\ \mathcal{B}^T K & -\gamma_\infty^2 I & \mathcal{D}^T \\ \mathcal{C} & \mathcal{D} & -I \end{bmatrix} < 0$$

$$\mathcal{A} := \begin{pmatrix} A + B_2 D_c C_2 & B_2 C_c \\ B_c C_2 & A_c \end{pmatrix}$$

$$\mathcal{B} := \begin{pmatrix} B_1 + B_2 D_c D_{21} \\ B_c D_{21} \end{pmatrix}$$

$$\mathcal{C} := \begin{pmatrix} C_1 + D_{12} D_c C_2 & D_{12} C_c \end{pmatrix}$$

$$\mathcal{D} := D_{11} + D_{12} D_c D_{21}$$

The above inequality is a BMI that needs to be transformed into an LMI for resolution. For the problem to be solvable, it is imperative that, via the application of a filter in the signal path, the acceleration measurement signal D_{22} is constrained to be equal to

zero. Furthermore, the system must exhibit strict stability. By applying an appropriate congruence transformation, the previously mentioned BMI is converted into an LMI:

$$\left(K\,,\begin{pmatrix}A_c & B_c\\ C_c & D_c\end{pmatrix}\right)\;\rightarrow\;v=\left(\boldsymbol{X},\boldsymbol{Y},\begin{pmatrix}\widetilde{\boldsymbol{A}} & \widetilde{\boldsymbol{B}}\\ \widetilde{\boldsymbol{C}} & \widetilde{\boldsymbol{D}}\end{pmatrix}\right)$$

The matrix K is chosen in such a way that:

$$K=\begin{pmatrix}\boldsymbol{X} & M\\ M^T & *\end{pmatrix},\;K^{-1}=\begin{pmatrix}\boldsymbol{Y} & N\\ N^T & *\end{pmatrix}$$

The $\boldsymbol{X}$ and $\boldsymbol{Y}$ are nonsingular symmetric matrices with the same dimension as matrix A. These two matrices must be selected in a manner that satisfies the following conditions:

$$MN^T=I-\boldsymbol{XY}$$

in which M and N are nonsingular.

$$\mathcal{Y}=\begin{pmatrix}\boldsymbol{Y} & I\\ N^T & 0\end{pmatrix}$$

$$\mathcal{Y}^TK\mathcal{Y}=\begin{pmatrix}\boldsymbol{Y} & I\\ I & \boldsymbol{X}\end{pmatrix}$$

$$\mathcal{Y}^T(K\mathcal{A})\mathcal{Y}:=\begin{pmatrix}A\boldsymbol{Y}+B_2\widetilde{\boldsymbol{C}} & A+B_2\widetilde{\boldsymbol{D}}C_2\\ \widetilde{\boldsymbol{A}} & \boldsymbol{X}A+\widetilde{\boldsymbol{B}}\boldsymbol{C}_2\end{pmatrix}$$

$$\mathcal{Y}^T(K\mathcal{B}):=\begin{pmatrix}B_1+B_2\widetilde{\boldsymbol{D}}D_{21}\\ \boldsymbol{X}B_1+\widetilde{\boldsymbol{B}}D_{21}\end{pmatrix}$$

$$\mathcal{Y}^T\mathcal{C}:=\begin{pmatrix}C_1\boldsymbol{Y}+D_{12}\widetilde{\boldsymbol{C}} & C_1+D_{12}\widetilde{\boldsymbol{D}}C_2\end{pmatrix}$$

Using the aforementioned transformations, the LMI associated with H_∞ will be as follows:

$$\begin{pmatrix}A\boldsymbol{X}+\boldsymbol{X}A^T+B_2\widetilde{\boldsymbol{C}}+\widetilde{\boldsymbol{C}}^TB_2^T & * & * & *\\ \widetilde{\boldsymbol{A}}+A^T+C_2^T\widetilde{\boldsymbol{D}}^TB_2^T & \boldsymbol{Y}A+A^T\boldsymbol{Y}+\widetilde{\boldsymbol{B}}C_2+C_2^T\widetilde{\boldsymbol{B}}^T & * & *\\ B_1^T+D_{21}^T\widetilde{\boldsymbol{D}}^TB_2^T & B_1^T\boldsymbol{Y}+D_{21}^T\widetilde{\boldsymbol{B}}^T & -\gamma_\infty I_{n_u} & *\\ C_1\boldsymbol{X}+D_{12}\widetilde{\boldsymbol{C}} & C_1+D_{12}\widetilde{\boldsymbol{D}}C_2 & D_{11}+D_{12}\widetilde{\boldsymbol{D}}D_{21} & -\gamma_\infty I_{n_y}\end{pmatrix}<0$$

$$\begin{pmatrix}\boldsymbol{X} & I_n\\ I_n & \boldsymbol{Y}\end{pmatrix}>0$$

The unknown parameters in this LMI are $\widetilde{\boldsymbol{D}}$, $\widetilde{\boldsymbol{C}}$, $\widetilde{\boldsymbol{B}}$, $\widetilde{\boldsymbol{A}}$, $\boldsymbol{Y}$, $\boldsymbol{X}$. Ultimately, the control variables will be computed based on the following equations:

$$\begin{cases}\widetilde{\boldsymbol{D}}=D_c\\ \widetilde{\boldsymbol{C}}=D_cC_2X+C_cM^T\\ \widetilde{\boldsymbol{B}}=YB_2D_c+NB_c\\ \widetilde{\boldsymbol{A}}=YAX+YB_2D_cC_2X+NB_cC_2X+YB_2C_cM^T+NA_cM^T\end{cases}$$

References

1. Badri, P.; Amini, A.; Sojoodi, M. Robust fixed-order dynamic output feedback controller design for nonlinear uncertain suspension system. *Mech. Syst. Signal Process.* **2016**, *80*, 137–151. [CrossRef]
2. Ma, M.; Chen, H. Constrained H2 control of active suspensions using LMI optimization. In Proceedings of the 2006 Chinese Control Conference, Harbin, China, 7–11 August 2006.
3. Viadero-Monasterio, F.; Boada, B.; Boada, M.; Díaz, V. H_∞ Dynamic output feedback control for a networked control active suspension system under actuator faults. *Mech. Syst. Signal Process.* **2022**, *162*, 108050. [CrossRef]
4. Sun, W.; Gao, H.; Yao, B. Adaptive robust vibration control of full-car active suspensions with electrohydraulic actuators. *IEEE Trans. Control. Syst. Technol.* **2013**, *21*, 2417–2422. [CrossRef]
5. Zhang, H.; Zhang, X.; Wang, J. Robust gain-scheduling energy-to-peak control of vehicle lateral dynamics stabilisation. *Veh. Syst. Dyn.* **2014**, *52*, 309–340. [CrossRef]
6. Jin, X.; Wang, J.; Sun, S.; Li, S.; Yang, J.; Yan, Z. Design of constrained robust controller for active suspension of in-wheel-drive electric vehicles. *Mathematics* **2021**, *9*, 249. [CrossRef]
7. Akbari, A.; Lohmann, B. Output feedback H∞/GH2 preview control of active vehicle suspensions: A comparison study of LQG preview. *Veh. Syst. Dyn.* **2010**, *48*, 1475–1494. [CrossRef]
8. Akbari Alvanagh, A. Multi-Objective H_Infinity/GH_2 Preview Control of Active Vehicle Suspensions. Ph.D. Dessertation, Technische Universität München, München, Germany, 2009.
9. Youn, I.; Khan, M.; Uddin, N.; Youn, E.; Tomizuka, M. Road disturbance estimation for the optimal preview control of an active suspension systems based on tracked vehicle model. *Int. J. Automot. Technol.* **2017**, *18*, 307–316. [CrossRef]
10. Burl, J.B. *Linear Optimal Control: H (2) and H (Infinity) Methods*; Addison-Wesley Longman Publishing Co., Inc.: Boston, MA, USA, 1998.
11. Jurisch, M. Vertical trajectory planning: An optimal control approach for active suspension systems in autonomous vehicles. *Veh. Syst. Dyn.* **2022**, *60*, 3788–3809. [CrossRef]
12. Malekshahi, A.; Mirzaei, M. Designing a non-linear tracking controller for vehicle active suspension systems using an optimization process. *Int. J. Automot. Technol.* **2012**, *13*, 263–271. [CrossRef]
13. Saglam, F.; Unlusoy, Y.S. Adaptive ride comfort and attitude control of vehicles equipped with active hydro-pneumatic suspension. *Int. J. Veh. Des.* **2016**, *71*, 31–51. [CrossRef]
14. Sun, W.; Pan, H.; Gao, H. Filter-based adaptive vibration control for active vehicle suspensions with electrohydraulic actuators. *IEEE Trans. Veh. Technol.* **2015**, *65*, 4619–4626. [CrossRef]
15. Mousavi, Y.; Alfi, A.; Kucukdemiral, I.B.; Fekih, A. Tube-based model reference adaptive control for vibration suppression of active suspension systems. *IEEE/CAA J. Autom. Sin.* **2022**, *9*, 728–731. [CrossRef]
16. Al Aela, A.M.; Kenne, J.-P.; Angue Mintsa, H. A novel adaptive and nonlinear electrohydraulic active suspension control system with zero dynamic tire liftoff. *Machines* **2020**, *8*, 38. [CrossRef]
17. Liu, L.; Zhu, C.; Liu, Y.-J.; Wang, R.; Tong, S. Performance improvement of active suspension constrained system via neural network identification. *IEEE Trans. Neural Netw. Learn. Syst.* **2022**, *34*, 7089–7098. [CrossRef] [PubMed]
18. Wang, J.; Zhang, H.; Ma, K.; Liu, Z.; Chen, C. Neural adaptive self-triggered control for uncertain nonlinear systems with input hysteresis. *IEEE Trans. Neural Netw. Learn. Syst.* **2021**, *33*, 6206–6214. [CrossRef]
19. Na, J.; Huang, Y.; Wu, X.; Su, S.-F.; Li, G. Adaptive finite-time fuzzy control of nonlinear active suspension systems with input delay. *IEEE Trans. Cybern.* **2019**, *50*, 2639–2650. [CrossRef] [PubMed]
20. Khan, A.H.; Li, S.; Chen, D.; Liao, L. Tracking control of redundant mobile manipulator: An RNN based metaheuristic approach. *Neurocomputing* **2020**, *400*, 272–284. [CrossRef]
21. Khan, A.H.; Li, S.; Luo, X. Obstacle avoidance and tracking control of redundant robotic manipulator: An RNN-based metaheuristic approach. *IEEE Trans. Ind. Inform.* **2019**, *16*, 4670–4680. [CrossRef]
22. Han, S.-Y.; Dong, J.-F.; Zhou, J.; Chen, Y.-H. Adaptive fuzzy PID control strategy for vehicle active suspension based on road evaluation. *Electronics* **2022**, *11*, 921. [CrossRef]
23. Al Aela, A.M.; Kenne, J.-P.; Mintsa, H.A. Adaptive neural network and nonlinear electrohydraulic active suspension control system. *J. Vib. Control.* **2022**, *28*, 243–259. [CrossRef]
24. Na, J.; Huang, Y.; Wu, X.; Liu, Y.-J.; Li, Y.; Li, G. Active suspension control of quarter-car system with experimental validation. *IEEE Trans. Syst. Man Cybern. Syst.* **2021**, *52*, 4714–4726. [CrossRef]
25. Joseph, S.B.; Dada, E.G.; Abidemi, A.; Oyewola, D.O.; Khammas, B.M. Metaheuristic algorithms for PID controller parameters tuning: Review, approaches and open problems. *Heliyon* **2022**, *8*, e09399. [CrossRef] [PubMed]
26. Mozaffari, A.; Doosthoseini, A.; Azad, N.L. Predictive control of suspension systems through combining dynamic matrix and constrained variable structure controllers. *J. Dyn. Syst. Meas. Control.* **2016**, *138*, 121007. [CrossRef]
27. Rodriguez-Guevara, D.; Favela-Contreras, A.; Beltran-Carbajal, F.; Sotelo, C.; Sotelo, D. An MPC-LQR-LPV controller with quadratic stability conditions for a nonlinear half-car active suspension system with electro-hydraulic actuators. *Machines* **2022**, *10*, 137. [CrossRef]
28. Rodriguez-Guevara, D.; Favela-Contreras, A.; Beltran-Carbajal, F.; Sotelo, D.; Sotelo, C. Active suspension control using an MPC-LQR-LPV controller with attraction sets and quadratic stability conditions. *Mathematics* **2021**, *9*, 2533. [CrossRef]

29. Chen, G.; Jiang, Y.; Tang, Y.; Xu, X. Revised adaptive active disturbance rejection sliding mode control strategy for vertical stability of active hydro-pneumatic suspension. *ISA Trans.* **2023**, *132*, 490–507. [CrossRef]
30. Rath, J.J.; Defoort, M.; Sentouh, C.; Karimi, H.R.; Veluvolu, K.C. Output-constrained robust sliding mode based nonlinear active suspension control. *IEEE Trans. Ind. Electron.* **2020**, *67*, 10652–10662. [CrossRef]
31. Hrovat, D. Survey of advanced suspension developments and related optimal control applications. *Automatica* **1997**, *33*, 1781–1817. [CrossRef]
32. Esmaeili, J.S.; Akbari, A.; Karimi, H.R. Load-dependent LPV/H2 output-feedback control of semi-active suspension systems equipped with MR damper. *Int. J. Veh. Des.* **2015**, *68*, 119–140. [CrossRef]
33. Esmaeili, J.S.; Akbari, A.; Mirzaei, M. LPV H2 control of semi-active suspensions. In Proceedings of the 2nd International Conference on Control, Instrumentation and Automation (ICCIA 2011), Shiraz, Iran, 27–29 December 2011.
34. Jing, H.; Li, X.; Karimi, H. Output-feedback based H∞ control for active suspension systems with control delay. *IEEE Trans. Ind. Electron.* **2014**, *61*, 436–446.
35. Gáspár, P.; Szaszi, I.; Bokor, J. Design of robust controllers for active vehicle suspension using the mixed μ synthesis. *Veh. Syst. Dyn.* **2003**, *40*, 193–228. [CrossRef]
36. Jin, X.; Wang, J.; He, X.; Yan, Z.; Xu, L.; Wei, C.; Yin, G. Improving vibration performance of electric vehicles based on in-wheel motor-active suspension system via robust finite frequency control. *IEEE Trans. Intell. Transp. Syst.* **2023**, *24*, 1631–1643. [CrossRef]
37. Poussot-Vassal, C.; Sename, O.; Dugard, L.; Gaspar, P.; Szabo, Z.; Bokor, J. A new semi-active suspension control strategy through LPV technique. *Control. Eng. Pract.* **2008**, *16*, 1519–1534. [CrossRef]
38. Boyd, S.; El Ghaoui, L.; Feron, E.; Balakrishnan, V. *Linear Matrix Inequalities in System and Control Theory*; Society for Industrial and Applied Mathematics: Philadelphia, PA, USA, 1994.
39. Skogestad, S.; Postlethwaite, I. *Multivariable Feedback Control: Analysis and Design*; John Wiley & Sons: Hoboken, NJ, USA, 2005.
40. Gahinet, P.; Nemirovskii, A.; Laub, A.J.; Chilali, M. The LMI control toolbox. In Proceedings of the 1994 33rd IEEE Conference on Decision and Control, Lake Buena Vista, FL, USA, 14–16 December 1994; IEEE: Piscataway, NJ, USA, 1994.
41. Scherer, C.; Weiland, S. *Linear Matrix Inequalities in Control*; Lecture Notes; Dutch Institute for Systems and Control: Delft, The Netherlands, 2000; Volume 3.
42. Scherer, C.; Gahinet, P.; Chilali, M. Multiobjective output-feedback control via LMI optimization. *IEEE Trans. Autom. Control.* **1997**, *42*, 896–911. [CrossRef]
43. Jang, J.-S. ANFIS: Adaptive-network-based fuzzy inference system. *IEEE Trans. Syst. Man Cybern.* **1993**, *23*, 665–685. [CrossRef]